The SDSU Broadband Ground-Motion Generation Module BBtoolbox Version 1.5

by Kim Olsen and Rumi Takedatsu

Online Material: Descriptions of validation events and scenarios; fixed and region-dependent parameters; additional goodness-of-fit plots for ground-motion prediction equations (GMPEs) versus data, simulations versus GMPEs, and pseudospectral accelerations (PSA) bias versus distance; and comparison of rupture models with associated PSA bias and time histories for Landers.

INTRODUCTION

The Southern California Earthquake Center (SCEC) has completed phase 1 of its Broadband Platform (BBP) ground-motion simulation results, evaluating the potential applications for engineering of the resulting 0.01–10 s pseudospectral accelerations (PSAs) generated by five different methods. The exercise included part A, in which the methods were evaluated based on the bias of simulation results to observations for 12 well-recorded historical earthquakes: 7 in the western United States, 2 in Japan, and 3 in the eastern United States/Canada. In addition, part B evaluated simulation results for M_w 5.5, 6.2, and 6.6 scenarios at 20 and 50 km from the fault. The methods were assessed based on the bias of the median PSA for the 12 events in part A and on a specified acceptance criterion compared with Next Generation Attenuation-West (NGA-West) ground-motion prediction equations (GMPEs) in part B. The results were evaluated by the bias of mean PSA from simulations using 1D velocity models with V_S^{30} (average shear-wave velocity in the upper 30 m) = 863 m/s (see the electronic supplement of Goulet *et al.*, 2015) with respect to recorded data corrected for site effects. The part A events and part B scenarios are described in Ⓔ Tables S1 and S2 (available in the electronic supplement to this article), respectively.

One of the five methods evaluated was the Broadband Synthetics Generator Module BBtoolbox, a hybrid method combining deterministic low-frequency (LF) synthetics with high-frequency (HF) scatterograms (Mai *et al.*, 2010; Mena *et al.*, 2010). The LFs may be computed using deterministic or dynamic descriptions in 1D or 3D media. The HF scatterograms are generated for each component of motion based on the theory for multiple *S*-to-*S* scattering by Zeng *et al.* (1991, 1993). The scatterograms are based on user-specified site-scattering parameters and are partly based on the site-specific velocity structure. The seismic-scattering wave energy is realized to appear after the direct *P*-wave arrival time, which is found from 3D ray tracing (Hole, 1992). Finally, the scatterograms are convolved with an appropriate source time function. It is assumed that the scattering operators and moment release originate throughout the fault but start at the hypocenter. The hybrid broadband seismograms are calculated in the frequency domain using a simultaneous amplitude- and phase-matching algorithm (Mai and Beroza, 2003). In the validation exercise, the LFs are generated using 50 source realizations from the kinematic source generator module by Graves and Pitarka (2015) on the SCEC BBP, through the standard rupture format (SRF), identical to those used by the Graves and Pitarka method.

BBtoolbox V1.4 (as described in Mai *et al.*, 2010, and Mena *et al.*, 2010) merges LFs and HFs by adjusting the level of the HF acceleration spectra to the corresponding LF spectral value at a specified merging frequency. This procedure was introduced in part to ensure continuity in the broadband synthetics at the merging frequency. Although this approach tends to work well for LFs calculated in well-constrained 3D structural models, the results for simplified 1D velocity models averaged over a region were found to generate, at times, strongly biased HF PSA levels. In addition, the scaling of the HFs to the LFs carries any directivity effects from the LFs to arbitrarily high frequencies, where observational support is lacking. In addition, the shape of the existing source time functions often times did not capture the shape of the PSA trends. The bias introduced by these issues did not permit BBtoolbox V1.4 to pass the SCEC validation phase 1.

To obtain more accurate broadband synthetics, as defined by the SCEC validation phase 1 targets and respective 1D Green's functions (GFs), we generated BBtoolbox V1.5. This article describes the changes that were made to BBtoolbox V1.4 to obtain V1.5 and presents the improved results that enabled BBtoolbox V1.5 to pass the validation.

BBTOOLBOX V1.5

BBtoolbox V1.5 contains two significant changes, as compared to V1.4. The first modification relates to the merging procedure, in which BBtoolbox V1.5 scales (or anchors) the HFs to a theoretical spectral level, rather than to the level of the LFs. The merging procedure for V1.5 involves the computation of a

doi: 10.1785/0220140102

single spectral scaling value for each station, because the merging between LFs and HFs is performed in the frequency domain. This scaling value is in part based on Graves and Pitarka (2010), with many similarities and some differences, which are described below.

Graves and Pitarka (2010) calculate the spectral acceleration amplitude as

$$A_i(f) = C_{ij} S_i(f) G_{ij}(f) P(f), \tag{1}$$

in which $C_{ij} = F_s R p_{ij}/(4\pi\rho_i\beta_i^3)$ is a radiation scale factor, with $F_s = 2$ accounting for the free surface amplification, Rp_{ij} is a conically averaged (P- and S-wave) radiation pattern term from the takeoff angle and focal mechanism, and ρ_i and β_i are density and shear-wave velocity in the middle of each subfault.

$$S_i(f) = m_i(M_0/N)(2\pi \times f)^2[1 + F(f/f_{ci})^2]^{-1} \tag{2}$$

is a source radiation term, in which $m_i = d_i\mu_i A_T/M_0$ is the average subfault moment calculated using the slip (d_i) and shear modulus (μ_i) of the ith subfault, as well as the total fault area A_T and the total scalar moment (M_0). $F = M_0/(N\,\text{strfac}\,\text{dl}^3)$ is a scaling factor for the subfaults, in which N is the number of subfaults, strfac is the Brune stress parameter, and dl is the average subfault dimension. $f_{ci} = c_0 V_{Ri}/(\alpha_T \pi \text{dl})$ and V_{Ri} are the corner frequency and rupture velocity, respectively, of the ith subfault, and α_T is a scale factor accounting for the fault dip (δ)-dependence of the ground motion. α_T is calculated as

$$\alpha_T = 0.82 \quad \text{for } \delta \le 55° \quad \text{and} \quad 1 \quad \text{for } \delta \ge 70°, \tag{3}$$

with a linear transition between dips of 55° and 70°. This calculation of α_T is slightly different from that of Graves and Pitarka (2010), based on comparisons of selected BBtoolbox V1.5 synthetics with those from GMPEs; also note the typos in Graves and Pitarka (2010, equation 12).

Graves and Pitarka calculate the path effect term $G_{ij}(f)$ of the jth ray from the ith subfault to the station as

$$G_{ij}(f) = I_i(f) \exp(-\pi f^{1-\text{fdec}} T/Q_0)/r_{ij}(x), \tag{4}$$

in which $I_i(f)$ is the impedance effect from the quarter-wavelength theory outlined by Boore and Joyner (1997), and $r_{ij}(x)$ is the total path length of the jth ray from the ith subfault to the receiver. $Q(f)$ is approximated as a power law $Q_0 f^{\text{fdec}}$, and T/Q_0 is approximated as $\Sigma t_{ijk}/q_k$, in which t_{ijk} is the travel time of the jth ray from the ith subfault to the station, $q_k = a\text{fac} + b\text{fac}\,\beta_k$, in which $a$fac and $b$fac are regionally dependent empirical constants and β_k is the shear-wave velocity of the kth layer, and the sum is over the stack of layers in the 1D crustal model.

At low frequencies, the acceleration spectra of the subfaults $A_i(f)$ in equation (1) sum coherently to the total spectrum as $A(f) = N\Sigma A_i(f)$, in which N is the sum of the subfaults. However, as shown by Joyner and Boore (1986), this summation becomes frequency dependent due to destructive interference of random phasing. More specifically, at the HF limit, we get

$$A(f) = (N^{1/2}/N)\Sigma A_i(f). \tag{5}$$

Although the HF amplitudes for Graves and Pitarka vary with frequency, we define a scaling of the HFs for BBtoolbox V1.5 based on equations (1)–(4) that applies to all frequencies larger than the merging frequency for a given source–station pair. This scaling value is calculated using $f = 50$ Hz in equations (1) and (2), a frequency sufficiently high to honor the criterion in equation (5). However, due to the scaling of the HFs by a single value averaged over the HF component, we use an additional average multiplicative factor of 1.4 in

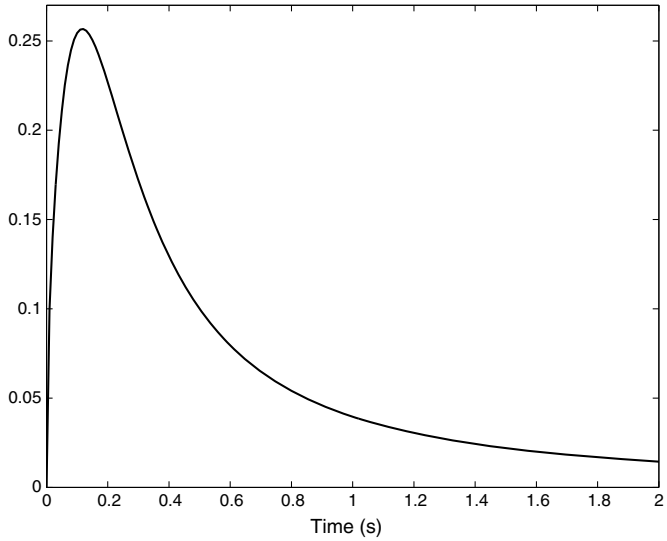

▲ **Figure 1.** Shape of the source time function convolved with the scatterograms in BBtoolbox V1.5.

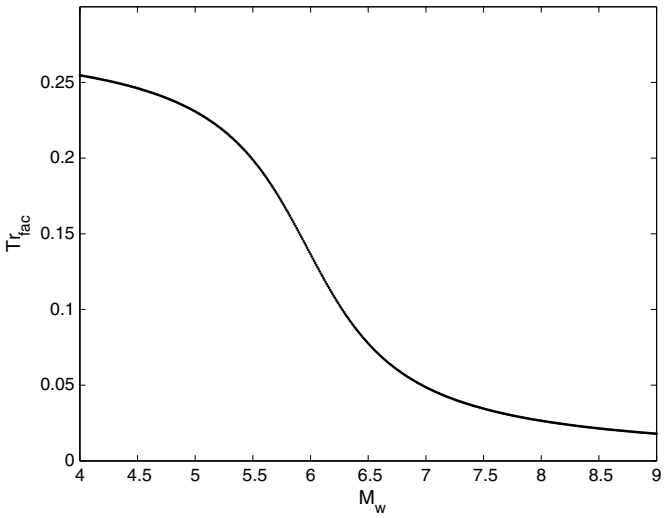

▲ **Figure 2.** M_w-dependent scaling factor for the rise time used for the source time function (see Fig. 1).

equation (5) to obtain an optimal performance as measured by the scenarios in parts A and B. BBtoolbox V1.5 uses $f = 1$ Hz in equation (4) and incorporates $Q = Q_0 f^{fdec}$ into the scatterograms for all frequencies above the merging frequency. We extract fault and rupture parameters used to calculate the scaling directly from the kinematic source description generated in SRF from the Graves and Pitarka rupture generator implemented on the BBP. Finally, BBtoolbox V1.5 uses a magnitude-dependent merging frequency, 1 Hz for $M_w \geq 5.25$ and 2 Hz for $M_w \leq 4.75$, with a linear transition of the merging frequency between M_w 4.75 and 5.25.

We approximate the distance between subfaults and receivers in equation (4), $r_{ij}(x)$ as a straight path for source–station distances ≤ 200 km, which is the range used for most scenarios in the validation. However, for source–receiver distances beyond 200 km, which was considered for the eastern scenario Mineral (up to 300 km) due to a sparse data set, a revised distance term of $r_{ij}^{1.1}(x)$ was used to obtain an acceptable fit to data. This increases the source–station distance for long-range wave propagation, which may be explained by the development of multiply reflected ray paths inside the crust. Further tests are needed to examine this issue and to determine whether it is specific to eastern North America events.

The other change to BBtoolbox V1.4 to obtain V1.5 is the shape of the source time function used for convolution with the scattering GFs. Mai *et al.* (2010) and Mena *et al.* (2010)

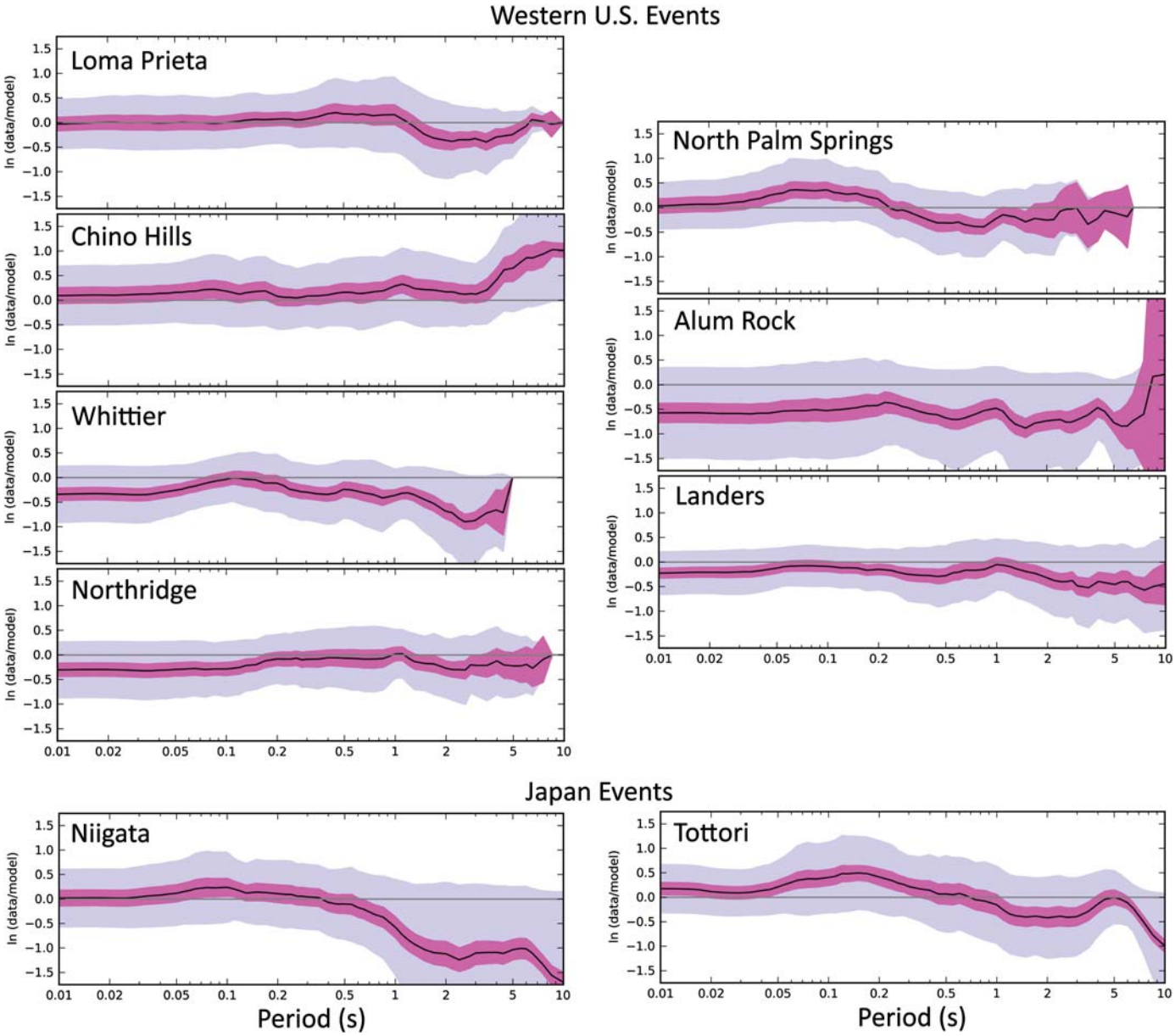

▲ **Figure 3.** Combined (50 realization) pseudospectral acceleration (PSA) bias (ln [data/model]) for the seven western United States and two Japan events. Thick line depicts the median, purple shading shows the 95% confidence interval, and light blue shading indicates the standard deviation.

used BBtoolbox V1.4 with the source time function defined by Dreger *et al.* (2007). However, a different source time function has been implemented in V1.5, with its rise time scaled as a function of M_w; this provides a better fit of PSA curves between synthetics and data, and has been used exclusively for all scenarios in the validation. The functional form of this source time function is

$$S(t) = t^{0.5}/[1 + (t/t_0)^2], \quad (6)$$

in which $t_0 = T_{rfac} \times T_r$, $T_r = \alpha_T\, 2.03 \times M_0^{1/3}/10^9$, with M_0 in dyn·cm (see Fig. 1). T_{rfac} is an M_w-dependent rise-time scaling factor given by

$$T_{rfac} = 0.141 - 0.09 \tan^{-1}(1.6\, M_w - 9.55), \quad (7)$$

and α_T is given in equation (3) (see Fig. 2). Because T_{rfac} scales the ground-motion amplitudes and appears strongly dependent on earthquake size, these relations should be used with caution outside the range tested here (M_w 4.6–7.22).

RESULTS

BBtoolbox V1.5 was validated on the BBP for the SCEC validation phase 1. The parameters used in the validation (both fixed and region specific) are listed in Ⓔ Tables S3 and S4, respectively. Figure 3 shows bias of PSA for an ensemble of 50 realizations for the seven western United States and two Japan events. In general, the fits are good, except the relatively large overprediction for Alum Rock for most periods. This bias is likely due to a large negative event term (average data residuals), supported by similar overprediction by leading GMPEs (see Ⓔ Fig. S1). The fits are generally better for shorter periods (< 1 s), as there is some tendency to overpredict for the longer periods (> 1 s). The bias for the eastern United States/Canadian events is shown in Figure 4. The overall best fits for a constant stress parameter (strfac in equation 2) are obtained for 350 bars (Fig. 4, left). However, a slightly improved fit (for Mineral and Saguenay) is obtained when assuming a depth-dependent value of the stress parameter of the following form

$$\text{strfac} = 6.25\, Z_{tor} + 265 \text{ bars}, \quad (8)$$

generating values of strfac of 302 bars for Mineral, 342 bars for Riviere-du-Loup, and 399 bars for Saguenay (see Fig. 4, right). Here, Z_{tor} is the depth to the top of the rupture. Although some evidence of a depth-dependent stress parameter for eastern North America has been found (Boatwright and MacDonald, 2012), such a trend is still uncertain. Ⓔ Table S1 provides goodness-of-fit (GOF) values binned for various period and distance ranges, as well as the rupture mechanism for the part A validation results generated by BBtoolbox V1.5.

The performance of the San Diego State University (SDSU) module for part B of the validation is shown in Figure 5 for the northern California 1D velocity model

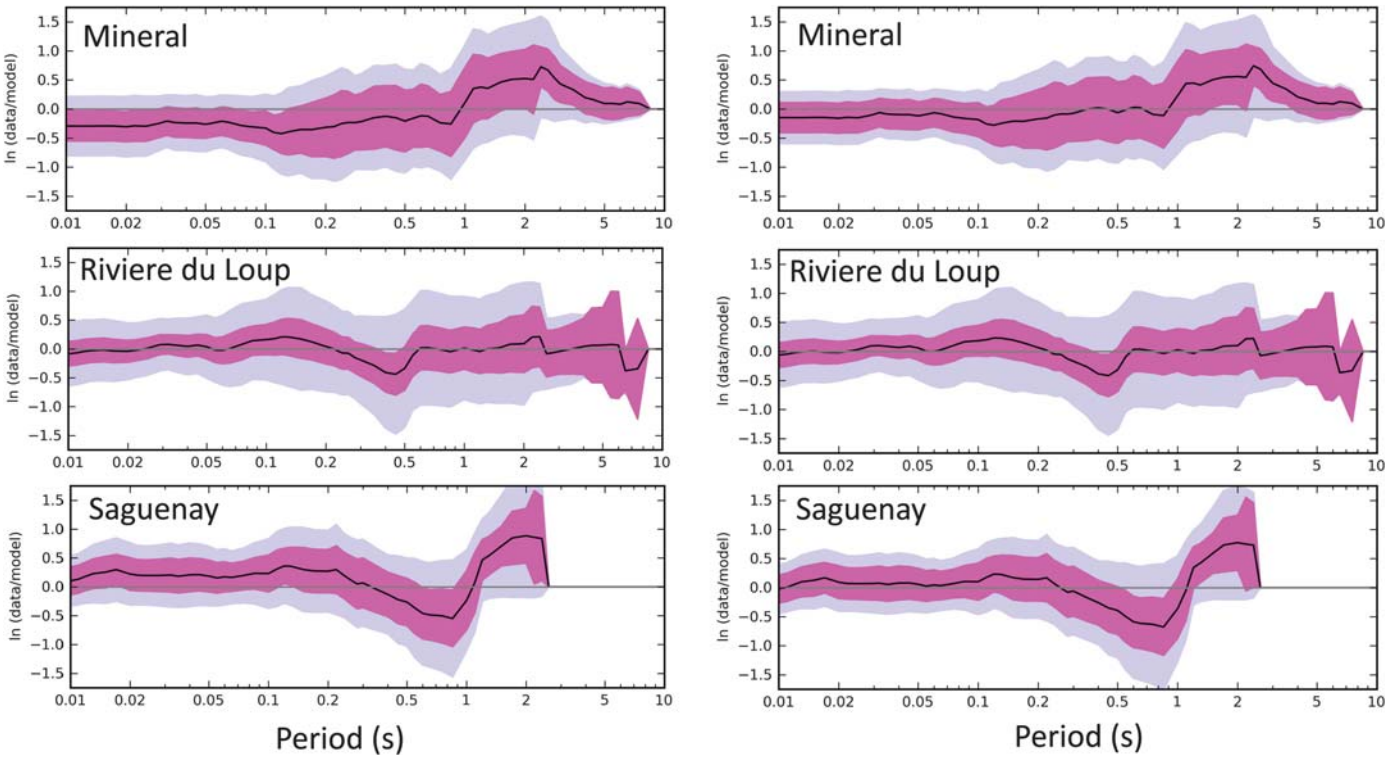

▲ **Figure 4.** Combined (50 realization) PSA bias for the three eastern United States/Canadian events. Results for stress parameter strfac (left) fixed at 350 bars and (right) depth dependent. The thick line depicts the median, purple shading shows the 95% confidence interval, and light blue shading indicates the standard deviation.

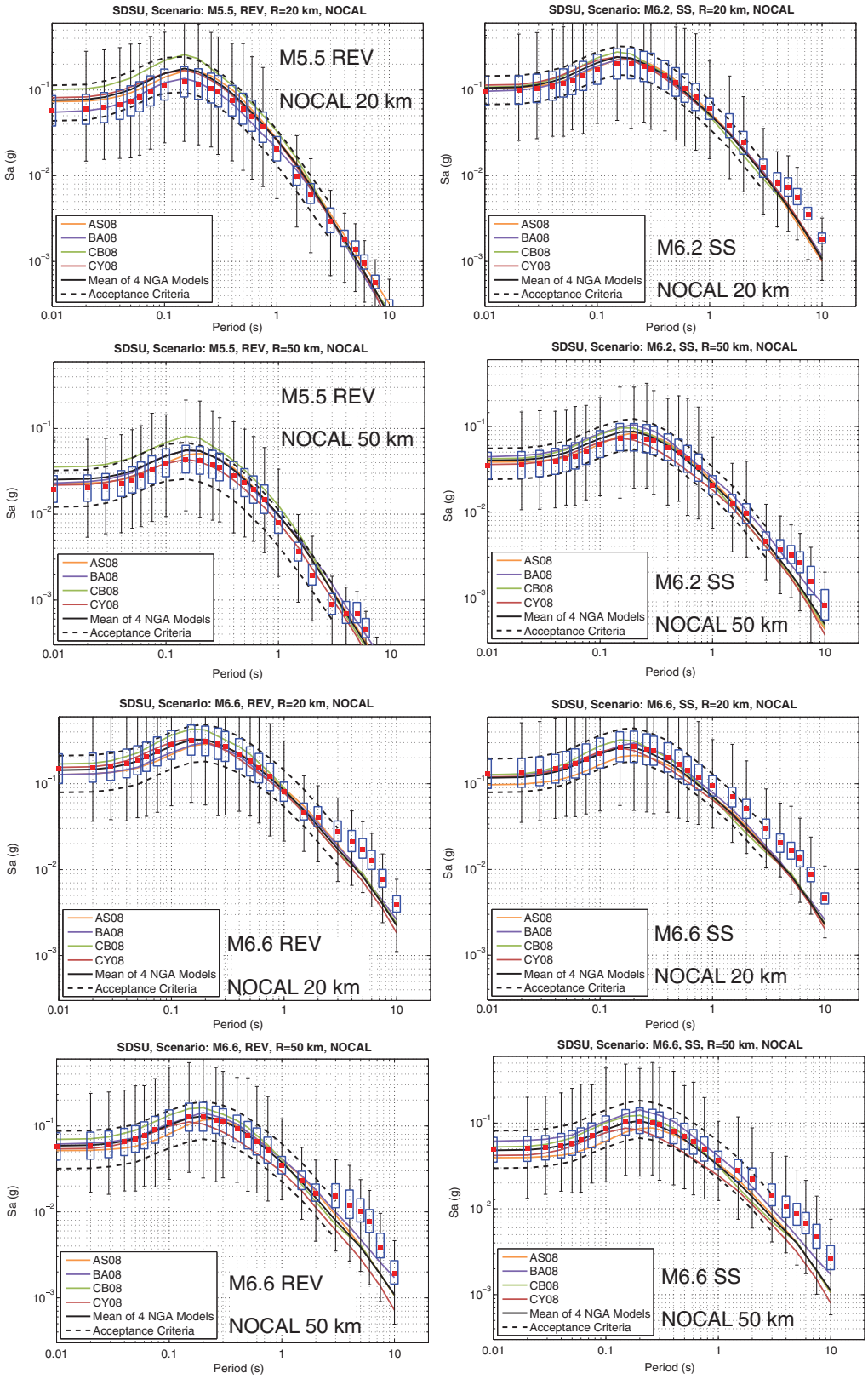

▲ **Figure 5.** Part B of the validation comparing PSAs for 50 realization ensemble synthetics against leading ground-motion prediction equations for M_w 5.5, 6.2, and 6.6 scenarios. The models are AS08, Abrahamson and Silva, 2008; BA08, Boore and Atkinson, 2008; CB08, Campbell and Bozorgnia, 2008; and CY08, Chiou and Youngs, 2008. NOCAL refers to the northern California 1D velocity model. The plots show the mean (squares) and standard deviation (boxes), whereas error bars show extrema for all realizations.

Table 1
Goodness-of-Fit (GOF) Summary for San Diego State University (SDSU) Validation Results (Natural Log of Observed-PSA/ Predicted-PSA) Binned by Distance, PSA Period, and Event Mechanism.

	Event (M_w,Mechanism)	SDSU 0.01–0.1 s		SDSU 0.1–1 s		SDSU 1–3 s		SDSU >3 s	
R_{rup} = (0-5) km	Chino Hills (5.39, ROBL)								
	Alum Rock (5.45, SS)	−0.65	0.65	−0.78	0.78	−1.32	1.32	−1.05	1.05
	Whittier Narrows (5.89, REV)								
	North Palm Springs (6.12, ROBL)	0.36	0.36	0.22	0.32	−0.51	0.51	−0.95	0.95
	Tottori (6.59, SS)	−0.40	0.40	0.40	0.51	−0.13	0.21	−0.31	0.31
	Niigata (6.65, REV)								
	Northridge (6.73, REV)								
	Loma Prieta (6.94, ROBL)	0.19	0.33	0.29	0.37	−0.12	0.53	−0.39	0.39
	Landers (7.22, SS)	0.92	0.92	0.45	0.45	0.53	0.53	0.44	0.44
	Riviere-du-Loup (4.6 REV)								
	Mineral (5.68 REV)								
	Saguenay (5.81 REV)								
	Average CA	0.20	0.48	0.13	0.44	−0.28	0.66	−0.24	0.54
	Average CENA								
	Average ALL	0.11	0.47	0.16	0.45	−0.26	0.60	−0.25	0.49
R_{rup} = (5-20) km	Chino Hills (5.39, ROBL)	0.17	0.28	0.29	0.38	0.65	0.65	0.84	0.84
	Alum Rock (5.45, SS)	−0.13	0.25	−0.03	0.38	−0.27	0.60	−0.17	0.68
	Whittier Narrows (5.89, REV)	−0.28	0.43	−0.16	0.40	−0.54	0.55	−1.01	1.01
	North Palm Springs (6.12, ROBL)	−0.11	0.33	−0.17	0.41	−0.30	0.65	−0.05	0.24
	Tottori (6.59, SS)	−0.29	0.32	0.08	0.38	−0.01	0.49	0.04	0.44
	Niigata (6.65, REV)	−0.15	0.52	−0.01	0.44	−0.53	0.81	−0.55	0.68
	Northridge (6.73, REV)	−0.06	0.37	0.16	0.42	−0.14	0.35	−0.10	0.32
	Loma Prieta (6.94, ROBL)	0.18	0.35	0.20	0.39	−0.32	0.40	−0.25	0.28
	Landers (7.22, SS)	−0.29	0.66	−0.02	0.54	−0.36	0.51	−0.85	0.85
	Riviere-du-Loup (4.6 REV)	−0.02	0.35	0.13	1.17	0.57	1.02	1.20	1.20
	Mineral (5.68 REV)	−0.66	0.66	−0.68	0.68	−0.23	0.23	−0.25	0.25
	Saguenay (5.81 REV)								
	Average CA	−0.06	0.37	0.05	0.41	−0.21	0.48	−0.07	0.51
	Average CENA	−0.24	0.45	−0.14	1.01	0.25	0.71	0.84	0.96
	Average ALL	−0.09	0.38	0.04	0.43	−0.19	0.52	−0.10	0.53
R_{rup} = (20-70) km	Chino Hills (5.39, ROBL)	0.01	0.47	−0.02	0.50	0.10	0.47	0.55	0.63
	Alum Rock (5.45, SS)	−0.72	0.80	−0.70	0.79	−0.81	0.86	−0.55	0.58
	Whittier Narrows (5.89, REV)	−0.27	0.43	−0.25	0.51	−0.51	0.61	−0.49	0.49
	North Palm Springs (6.12, ROBL)	0.30	0.52	−0.01	0.50	−0.15	0.42	−0.43	0.43
	Tottori (6.59, SS)	0.29	0.44	−0.02	0.59	−0.62	0.70	−0.44	0.57
	Niigata (6.65, REV)	0.04	0.43	−0.10	0.55	−0.95	1.07	−1.09	1.13
	Northridge (6.73, REV)	−0.54	0.55	−0.37	0.46	−0.22	0.53	−0.33	0.80
	Loma Prieta (6.94, ROBL)	−0.33	0.43	−0.18	0.42	−0.45	0.57	−0.18	0.36
	Landers (7.22, SS)	−0.27	0.35	−0.27	0.44	−0.55	0.64	−0.73	0.75
	Riviere-du-Loup (4.6 REV)	0.09	0.47	−0.08	0.60	−0.10	0.63	−0.25	0.30
	Mineral (5.68 REV)	−0.16	0.31	−1.18	1.19	−0.05	1.00	−0.07	0.10
	Saguenay (5.81 REV)	0.25	0.35	−1.33	1.33	−1.98	1.98		
	Average CA	−0.25	0.50	−0.26	0.52	−0.38	0.59	−0.35	0.62
	Average CENA	0.08	0.44	−0.34	0.75	−0.11	0.69	−0.23	0.28
	Average ALL	−0.15	0.49	−0.23	0.55	−0.45	0.66	−0.54	0.72
R_{rup} = (70-300) km	Chino Hills (5.39, ROBL)	0.31	0.55	0.31	0.60	0.19	0.73	0.58	0.91
	Alum Rock (5.45, SS)	−0.54	0.80	−0.48	0.77	−0.85	0.86	−0.86	0.86
	Whittier Narrows (5.89, REV)								
	North Palm Springs (6.12, ROBL)	−0.23	0.26	−0.46	0.50	0.23	0.36		
	Tottori (6.59, SS)	0.36	0.51	0.51	0.67	−0.32	0.70	−0.31	0.58
	Niigata (6.65, REV)	0.22	0.62	0.02	0.63	−1.33	1.36	−1.49	1.50
	Northridge (6.73, REV)	−0.05	0.28	0.19	0.49	−0.32	0.56	−0.31	0.31
	Loma Prieta (6.94, ROBL)	0.54	0.54	0.74	0.77	0.51	0.92	0.03	0.62
	Landers (7.22, SS)	−0.08	0.21	−0.14	0.35	0.03	0.39	0.03	0.47
	Riviere-du-Loup (4.6 REV)	−0.07	0.38	0.04	0.63	0.24	1.00	0.58	0.58
	Mineral (5.68 REV)	−0.03	0.38	0.31	0.51	0.79	0.81	0.20	0.28
	Saguenay (5.81 REV)	0.03	0.38	0.10	0.49	0.50	0.62	−0.13	0.13
	Average CA	−0.01	0.48	0.01	0.57	−0.06	0.65	0.00	0.69
	Average CENA	−0.01	0.38	0.15	0.53	0.58	0.77	0.18	0.27
	Average ALL	0.08	0.49	0.12	0.59	−0.22	0.80	−0.52	0.86
Mechanism	Reverse (REV)	−0.11	0.45	−0.11	0.54	−0.42	0.76	−0.80	0.95
	Reverse-Oblique (ROBL)	0.10	0.45	0.07	0.49	−0.05	0.56	0.16	0.54
	Strike-Slip (SS)	−0.18	0.49	−0.16	0.57	−0.45	0.66	−0.40	0.61
	Normal (NM)								
Total	**Average CA**	−0.15	0.47	−0.13	0.50	−0.26	0.58	−0.20	0.60
	Average CENA	0.01	0.41	−0.08	0.66	0.28	0.74	0.09	0.33
	Average ALL	−0.07	0.46	−0.08	0.53	−0.33	0.67	−0.44	0.72

Two values are listed for each bin: (left) sum of GOF values, and (right) sum of absolute GOF values. The entries are shaded dark gray (–0.50 £ GOF £ 0.50), white (–0.70 £ GOF < –0.50 or 0.50 < GOF £ 0.70), and light gray (GOF < –0.70 or GOF > 0.70). ROBL, reverse oblique; SS, strike slip; REV, reverse; CENA, central and eastern North America; R_{rup}, nearest distance to rupture surface.

(see Ⓔ Fig. S2 for results using the southern California 1D model). Here, PSAs (0.01–10 s) for M_w 5.5, 6.2, and 6.6 scenarios are compared for simulations and leading GMPEs (see Goulet *et al.*, 2015, for definition of the acceptance criteria). The mean PSAs from the simulations obtained by the SDSU module show very good agreement with the GMPEs and fall within the applicable acceptance criteria for all scenarios' periods.

The validation results for the SDSU module were checked for bias from various parameters in the modeling. Ⓔ Figures S3–S15 show bias versus fault–station distance for the part A events. In addition, Table 1 lists GOF values binned by distance, PSA period, and event mechanism. The GOF values for BBtoolbox V1.5 generally fall within the green (considered passing the validation) and white entries (marginal acceptance) for PSA periods < 1 s and all mechanisms but tend to increase for longer periods. The table and plots indicate no obvious bias with respect to fault–station distance, PSA period, fault mechanism, dip, and magnitude. It is also encouraging to notice the rupture and slip pattern for the source realizations generating the best fits appear generally to be in better agreement with the kinematic inversion models (e.g., Ⓔ Fig. S16). Moreover, the computed broadband synthetics appear realistic (e.g., Ⓔ Fig. S17).

SUMMARY AND FUTURE WORK

The SDSU broadband Ground-Motion Generation Module BBtoolbox V1.5 was obtained from modifications to BBtoolbox V1.4 (Mai *et al.*, 2010; Mena *et al.*, 2010). The most significant modification is the anchoring of the HF spectral acceleration of the broadband time series to the LF component using a theoretical level calculated from the finite-fault source description and path effects. In addition, we introduced a new source time function for convolution with the HF scattering functions and a modified geometrical spreading factor for long-range wave propagation (at least for eastern United States/Canadian events).

Because of these modifications, BBtoolbox V1.5 passed the SCEC BBP phase 1 validation. No significant bias of the median PSA (0.01–10 s) with respect to distance, magnitude, fault mechanism, depth to the top of the fault, or PSA period was observed for the method using seven events in the western United States, two Japanese events, and three eastern United States/Canadian events, and the synthetic time histories appear realistic. Moreover, mean PSAs computed by BBtoolbox V1.5 were all within the acceptance level for all distances and PSA periods for four M_w 5.5–6.6 scenarios with respect to leading NGA-West GMPEs.

The long-period results for the SDSU (and thus for the Graves and Pitarka method) synthetics were found to overpredict the strong-motion data and GPMEs in several cases (see Figs. 3–5). Although the reason for this long-period trend has not been determined, possible explanations include the use of simplified 1D crustal GFs for the simulations that may be generating too coherent wave trains, source descriptions (including magnitude–fault area relation and rupture complexity), and the omission of near-fault plastic (nonlinear) effects, as pointed out by Roten *et al.* (2014).

Based on the performance in the validation exercise, we expect BBtoolbox V1.5 to work satisfactorily for forward simulation of earthquake scenarios with magnitudes between 4.5 and 7.22 for all PSA periods and source–station distances up to at least 200 km. However, it should be cautioned that the accuracy of the long-period (> 1 s) PSAs depends on the performance of the rupture generator and the 1D GFs and that larger magnitude events need further validation. We find that using magnitudes specified in NGA-West 2 for historical earthquakes and the definition of the fault area based on earthquake magnitude by Leonard (2010) are appropriate for the use of BBtoolbox V1.5. We caution that the aspect ratio of the fault should be chosen not to violate any available constraints on the seismogenic depth.

Ongoing and future efforts related to BBtoolbox V1.5 will include validations for magnitudes larger than those tested here (e.g., M_w 7.22), PSA variability for multiple realizations on a single event, and further calibration of the depth-dependent stress parameter scaling for eastern United States/Canadian events. Future development of the code will consider Fourier spectra in addition to PSA metrics.

ACKNOWLEDGMENTS

We are grateful for the comments from Jack Baker and an anonymous reviewer. This work was supported by Southern California Earthquake Center (SCEC), which is funded by National Science Foundation (NSF) Cooperative Agreement EAR-1033462 and U.S. Geological Survey Cooperative Agreement G12AC20038, as well as NSF Award OCI-1148493 (SI2-SSI). We acknowledge the Pacific Earthquake Engineering Research Center for providing the recorded data. The SCEC Contribution Number for this article is 1985.

REFERENCES

Abrahamson, N. A., and W. J. Silva (2008). Summary of the Abrahamson & Silva NGA ground-motion relations, *Earthq. Spectra* **24,** no. 1, 67–97.

Boatwright, J., and T. MacDonald (2012). The variation of Brune stress drop with hypocentral depth for moderate ($2.5 \le M \le 5.8$) earthquakes in northeastern North America, *abstract presented at the Annual Meeting of the Eastern Section of SSA*, Blacksburg, Virginia, 28–30 October 2012.

Boore, D. M., and G. M. Atkinson (2008). Ground-motion prediction equations for the average horizontal component of PGA, PGV, and 5%-damped PSA at spectral periods between 0.01 and 10.0 s, *Earthq. Spectra* **24,** no. 1, 99–138.

Boore, D. M., and W. B. Joyner (1997). Site amplifications for generic rock sites, *Bull. Seismol. Soc. Am.* **87,** no. 2, 327–341.

Campbell, K. W., and Y. Bozorgnia (2008). NGA ground motion model for the geometric mean horizontal component of PGA, PGV, PGD and 5% damped linear elastic response spectra for periods ranging from 0.01 to 10s, *Earthq. Spectra* **24,** no. 1, 139–171.

Chiou, B. S.-J., and R. R. Youngs (2008). An NGA model for the average horizontal component of peak ground motion and response spectra, *Earthq. Spectra* **24,** no. 1, 173–215.

Dreger, D., E. Tinti, and A. Cirella (2007). Slip velocity function parameterization for broadband ground motion simulation, *Seismol. Res. Lett.* **78,** no. 2, 308.

Goulet, C. A., N. A. Abrahamson, P. G. Somerville, and K. E. Wooddell (2015). The SCEC broadband platform validation exercise: Methodology for code validation in the context of seismic hazard analyses, *Seismol. Res. Lett.* **86,** no. 1, doi: 10.1785/0220140104.

Graves, R. W., and A. Pitarka (2010). Broadband ground-motion simulation using a hybrid approach, *Bull. Seismol. Soc. Am.* **100,** no. 5A, 2095–2123, doi: 10.1785/0120100057.

Graves, R. W., and A. Pitarka (2015). Refinements to the Graves and Pitarka (2010) broadband ground motion simulation method, *Seismol. Res. Lett.* **86,** no. 1, doi: 10.1785/0220140101.

Hole, J. A. (1992). Non-linear high resolution three-dimensional seismic travel time tomography, *J. Geophys. Res.* **97,** 6553–6562.

Joyner, W. B., and D. M. Boore (1986). On simulating large earthquakes by Green's function addition of smaller earthquakes, in *Earthquake Source Mechanics*, Maurice Ewing Series, S. Das, J. Boatwright, and C. H. Scholz (Editors), Vol. 6, American Geophysical Union, Washington, D.C., 269–274.

Leonard, M. (2010). Earthquake fault scaling: Self-consistent relating of rupture length, width, average displacement, and moment release, *Bull. Seismol. Soc. Am.* **100,** no. 5A, 1971–1988.

Mai, P. M., and G. C. Beroza (2003). A hybrid method for calculating near-source, broadband seismograms: Application to strong motion prediction, *Phys. Earth Planet. Int.* **137,** nos. 1/4, 183–199.

Mai, P. M., W. Imperatori, and K. B. Olsen (2010). Hybrid broadband ground-motion simulations: Combining long-period deterministic synthetics with high-frequency multiple *S*-to-*S* backscattering, *Bull. Seismol. Soc. Am.* **100,** no. 5A, 2124–2142, doi: 10.1785/0120080194.

Mena, B., P. M. Mai, K. B. Olsen, M. D. Purvance, and J. N. Brune (2010). Hybrid broadband ground-motion simulation using scattering Green's functions: Application to large-magnitude events, *Bull. Seismol. Soc. Am.* **100,** no. 5A, 2143–2162, doi: 10.1785/0120080318.

Roten, D., K. B. Olsen, S. M. Day, Y. Cui, and D. Fah (2014). Expected seismic shaking in Los Angeles reduced by San Andreas fault zone plasticity, *Geophys. Res. Lett.* **41,** no. 8, 2769–2777, doi: 10.1002/2014GL059411.

Zeng, Y. H., K. Aki, and T. L. Teng (1993). Mapping of the high-frequency source radiation for the Loma Prieta earthquake, California, *J. Geophys. Res.* **98,** no. B7, 11,981–11,993.

Zeng, Y. H., F. Su, and K. Aki (1991). Scattering wave energy propagation in a random isotropic scattering medium 1. Theory, *J. Geophys. Res.* **96,** no. B1, 607–619.

Kim Olsen
Rumi Takedatsu
Department of Geological Sciences
GMCS 231A
San Diego State University
5500 Campanile Drive
San Diego, California 92182 U.S.A.
kbolsen@mail.sdsu.edu

Published Online 17 December 2014